

# Giant acoustoelectric effect in GaAs/LiNbO<sub>3</sub> hybrids

Cite as: Appl. Phys. Lett. **73**, 2128 (1998); <https://doi.org/10.1063/1.122400>  
 Submitted: 26 May 1998 • Accepted: 11 August 1998 • Published Online: 29 October 1998

M. Rotter, A. Wixforth, W. Ruile, et al.



View Online



Export Citation

## ARTICLES YOU MAY BE INTERESTED IN

[Acoustically induced current flow in graphene](#)

Applied Physics Letters **100**, 133105 (2012); <https://doi.org/10.1063/1.3697403>

[Macroscopic acoustoelectric charge transport in graphene](#)

Applied Physics Letters **103**, 133101 (2013); <https://doi.org/10.1063/1.4822121>

[Flip-chip gate-tunable acoustoelectric effect in graphene](#)

Journal of Applied Physics **124**, 194302 (2018); <https://doi.org/10.1063/1.5047211>

 QBLOX



1 qubit

Shorten Setup Time  
**Auto-Calibration**  
**More Qubits**

Fully-integrated  
**Quantum Control Stacks**  
**Ultrastable DC to 18.5 GHz**  
 Synchronized <<1 ns  
 Ultralow noise



100s qubits

[visit our website >](#)



## Giant acoustoelectric effect in GaAs/LiNbO<sub>3</sub> hybrids

M. Rotter<sup>a)</sup> and A. Wixforth

*Sektion Physik der LMU, Universität München, D-80539 München, Germany*

W. Ruile, D. Bernklau, and H. Riechert

*Siemens AG, Corporate Technology, D-81730 München, Germany*

(Received 26 May 1998; accepted for publication 11 August 1998)

The acoustoelectric effect in a hybrid of a strong piezoelectric material and a semiconductor layer containing a two-dimensional electron system is investigated. Caused by the very strong interaction between a surface acoustic wave and the mobile carriers in the semiconductor, the acoustoelectric effect is very large as compared to other materials, which might be interesting for device applications. Moreover, the tunability of the sheet conductivity of the electron system enables us to tune the magnitude of the acoustoelectric effect over a wide range. We present experimental results for a GaAs/LiNbO<sub>3</sub> layered hybrid system at room temperature and describe our experimental findings quantitatively using a recently developed model calculation. © 1998 American Institute of Physics. [S0003-6951(98)01141-3]

The interaction between surface acoustic waves (SAW) and low-dimensional electron systems as confined in modern semiconductor layered systems has recently attracted a lot of attention. The sensitivity of the interaction to very low conductivities as well as the possibility to create dynamic superlattices in semiconductor structures makes it in particular interesting.<sup>1-3</sup> However, most of the semiconductors that can be used for the realization of low-dimensional electron systems are only weakly piezoelectric. Hence, the interaction between the SAW and the free carriers in the semiconductor is also very weak. Recently, we introduced a technique for the hybridization of semiconductor layered systems and strongly piezoelectric substrates, that propelled the strength of the interaction into a regime being interesting for high excitation phenomena, nonlinear effects, and also for future device applications.<sup>4</sup> Here, the large momentum transfer from the SAW to the free carriers in the semiconductor is of particular interest.

Surface acoustic waves on piezoelectric substrates are accompanied by a potential wave and electric fields originating from the materials polarization under mechanical deformation. These electric fields interact with mobile carriers in a two-dimensional electron system (2DES) in close vicinity of the surface. Consequently, the 2DES influences the propagation of the SAW; it changes the wave velocity and produces an attenuation of the wave. The change in SAW phase velocity  $v$  is given by<sup>1,2</sup>

$$\frac{v - v_0}{v_0} = \frac{\Delta v}{v_0} = \frac{K^2}{2} \frac{1}{1 + (\sigma/\sigma_m)^2}, \quad (1)$$

where  $K^2$  denotes the effective electromechanical coupling coefficient,  $\sigma$  is the sheet conductivity, and  $\sigma_m$  is a material constant. The velocity  $v_0$  is the SAW velocity on a free surface. This velocity change is accompanied by an attenuation of the wave intensity  $I = I_0 e^{-\Gamma x}$  along the beam path  $x$ , given by

$$\Gamma = K^2 \frac{\pi}{\lambda} \frac{\sigma/\sigma_m}{1 + (\sigma/\sigma_m)^2}, \quad (2)$$

where  $\lambda$  is the wavelength of the SAW. At  $\sigma = \sigma_m$ , the attenuation  $\Gamma$  reaches its maximum. Since the SAW carries a flux of momentum equal to  $1/v$  times the flux of energy, a loss of wave energy has to be accompanied by a proportional loss of momentum. This loss of momentum appears as a force on the electron system. This phenomenon is known as the acoustoelectric (ae) effect, which was first predicted by Parmenter<sup>5</sup> and identified by Weinreich for bulk materials.<sup>6</sup> For the special case of 2DES Fal'ko *et al.* and Esslinger *et al.*<sup>7</sup> showed that the ae current density  $j$  is given by

$$j = \sigma E - \Lambda Q. \quad (3)$$

Here,  $\Lambda$  represents the ae tensor which — for zero magnetic field — simply reduces to the mobility,  $\Lambda = \mu$ ;  $Q$  represents a “phonon pressure” being proportional to the wave intensity  $I$  and the attenuation  $\Gamma$ :

$$Q = \frac{I\Gamma}{v}. \quad (4)$$

It should be pointed out that this model only applies in the small signal limit, i.e., for negligible modulation of the carrier concentration by the SAW. In the low-power experiments presented here, this is guaranteed at least for  $\sigma \geq \sigma_m$ . As the attenuation  $\Gamma$  is proportional to the coupling coefficient [Eq. (2)], a high  $K^2$  would be desirable in order to yield a large ae effect. However, on GaAs where high quality 2DES can be defined, the coupling coefficient is rather low ( $K^2 = 6.4 \times 10^{-4}$ ). On 128° rotated YX cut of LiNbO<sub>3</sub>,  $K^2 = 0.056$  is nearly two orders of magnitude larger. However, semiconductor layers are very difficult to fabricate on LiNbO<sub>3</sub>. A solution to this problem is the quasimonolithical hybridization of a thin GaAs-layer system and the LiNbO<sub>3</sub>. This has been shown to be possible<sup>4</sup> using the epitaxial lift-off technology (ELO) originally developed by Yablonovitch *et al.*<sup>8</sup>

<sup>a)</sup>Electronic mail: markus.rotter@physik.uni-muenchen.de

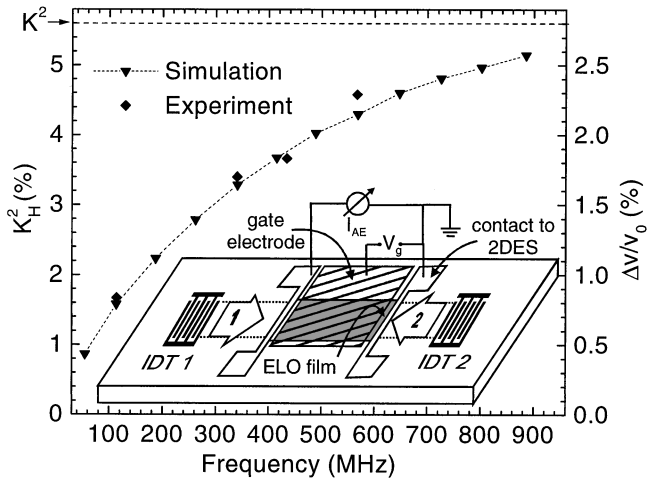


FIG. 1. Calculated and measured hybrid coupling coefficient  $K_H^2$  as a function of the SAW frequency. For higher frequencies, corresponding to smaller wavelength,  $K_H^2$  increases, eventually saturating at  $K^2$  of bare  $\text{LiNbO}_3$ . The inset shows the geometry of the hybrid chip.

Molecular beam epitaxy grown GaAs-based layered structures containing an AlAs sacrificial layer perfectly match the criteria for this hybridization. On top of the substrate and the sacrificial AlAs the active layers are grown, consisting of  $\text{Al}_{0.2}\text{Ga}_{0.8}\text{As}$  barrier material embedding a modulation-doped 12 nm  $\text{In}_{0.2}\text{Ga}_{0.8}\text{As}$  quantum well. On top of the structure, Ohmic contacts to the 2DES are defined. In the ELO process, the AlAs layer is then selectively etched away in hydrofluoric acid. Then the active layers, having a total thickness of  $0.5 \mu\text{m}$ , can be removed from the substrate and transferred onto the  $\text{LiNbO}_3$  chip with interdigital transducer structures (IDTs) for generating and detecting the SAW. The ELO film and substrate are tightly bonded by van der Waals forces. The distance between the quantum well and the  $\text{LiNbO}_3$  surface is just 32 nm, whereas the thickness of the barrier above the electron system is 450 nm. Subsequently, the ELO film is patterned and a gate electrode is formed (see the inset of Fig. 1).

When a gate voltage is applied between the gate electrode and the 2DES, the electron density in the quantum well is reduced, resulting in a change of conductivity. This influences the SAW intensity and the velocity of the wave. The magnitude of the influence is governed by the coupling coefficient  $K^2$ . However, when the 2DES is fully depleted, the electrical boundary condition for the surface wave is not exactly “open” because of the presence of a gate electrode at a finite distance of  $0.5 \mu\text{m}$  above the  $\text{LiNbO}_3$  surface. This reduces the velocity change of the SAW and thus the effective coupling coefficient. To account for this reduction, we introduce a new hybrid coupling coefficient  $K_H^2$  as a function of the SAW wavelength using a finite-element method for determining the SAW phase velocities. To check our calculations, we measured the velocity change in the hybrid via the phase shift of the rf signal in the delay line geometry for different frequencies. The comparison between simulation and measurement is shown in Fig. 1. For higher frequency, and therefore, smaller wavelength the screening of the SAW potential by the gate electrode becomes less significant, resulting in a higher  $K_H^2$ .

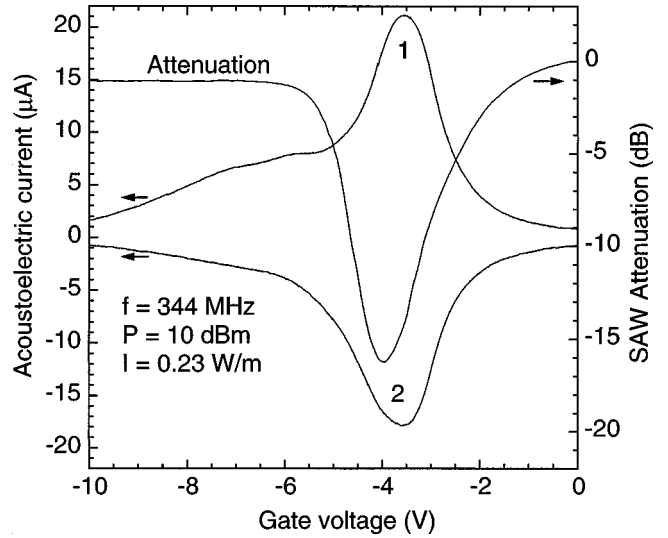


FIG. 2. Acoustoelectric current as a function of the gate bias at an applied power level of 10 dBm. Curves 1 and 2 correspond to the different SAW propagation directions as specified in the inset of Fig. 1. Reversing the SAW direction causes inversion of the ae current. The structure in the ae current traces for  $\sigma < \sigma_m$  is related to small inhomogeneities of the carrier concentration. We also show the measured attenuation  $\Gamma$  as a function of the applied gate voltage on this sample, displaying the correlation between attenuation  $\Gamma$  and ae effect.

This large hybrid coupling coefficient leads to a strong coupling between SAW and 2DES, and therefore, to a large acoustoelectric effect. In order to study this effect, we directly measure the SAW-induced current between the two Ohmic contacts (see Fig. 1) in a closed circuit (“shorted geometry”) and as a function of the gate bias. A continuous-wave rf signal is applied to one interdigital transducer for SAW generation. Figure 2 shows this ae current for the two different SAW propagation directions along the sample. If the SAW direction is reversed by applying the rf to the other transducer, the sign of the measured current is reversed as expected. We also display the measured attenuation  $\Gamma$  as a function of the applied gate voltage. It reaches a maximum at  $V_g = -4 \text{ V}$  corresponding to  $\sigma = \sigma_m$  and strongest interaction. The conductivity  $\sigma_m$  is approximately given by  $\sigma_m = v_0 \epsilon_0 (\sqrt{\epsilon_{xx}^T \epsilon_{zz}^T} + 1) = 2.1 \times 10^{-6} \Omega^{-1}$  for a frequency of  $f = 344 \text{ MHz}$ , with  $\epsilon_{xx}^T$  and  $\epsilon_{zz}^T$  denoting the dielectric constants of  $\text{LiNbO}_3$  at constant stress conditions. Employing this value for  $\sigma_m$ , the hybrid coupling coefficient  $K_H^2$ , and the hybrid velocities from the finite-element simulations, we achieve very good agreement between the measured attenuation and the theory according to Eqs. (1) and (2) in the hybrid systems.<sup>9</sup> Figure 2 clearly displays that the ae current also reaches its maximum around  $\sigma = \sigma_m$ , as expected from Eqs. (3) and (4).

For the “shorted geometry,” no ae field can build up ( $E=0$ ) and Eq. (3) yields an ae current density of

$$j_{sc} = -\Lambda Q = -\frac{\mu I \Gamma}{v}. \quad (5)$$

For a quantitative analysis of our experimental data all relevant quantities were evaluated separately: The transport parameters  $\mu$  and carrier concentration  $n_S$  of the 2DES were determined using a van der Pauw method. At  $V_g = 0 \text{ V}$  the room-temperature mobility turns out to be  $\mu = 3800 \text{ cm}^2/\text{V s}$ .

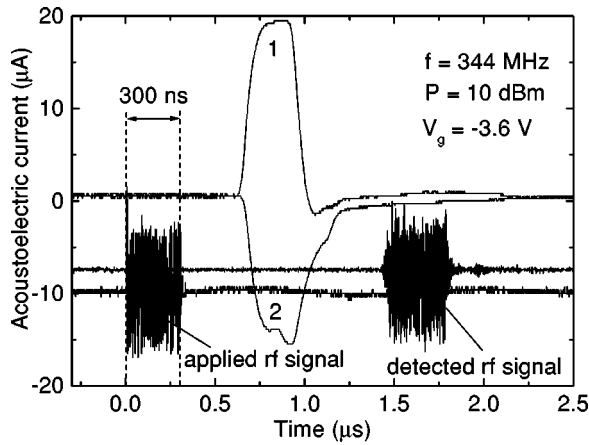


FIG. 3. Time-resolved measurement of the ae current employing SAW pulses ( $\tau=300$  ns). Again, traces 1 and 2 denote different SAW propagation directions. Oscilloscope traces of the applied and detected rf signals (noisy bursts) at the transducers are shown to elucidate the timing sequence of the signals. The current scale is calculated from the oscilloscope voltage drop at a resistance of 1 k $\Omega$ .

At conductivity  $\sigma=\sigma_m$  we obtain a mobility of  $\mu=1000$  cm<sup>2</sup>/V s and a carrier concentration of  $n_s=1.2\times 10^{10}$ cm<sup>-2</sup>. As the sample is symmetric with respect to the axis perpendicular to the SAW propagation direction, we estimate the acoustic intensity  $I$  in the center of the film by subtracting half of the total insertion loss ( $V_g=0$  V) from the applied rf power to the transducer. With a transducer aperture of  $A=800$   $\mu$ m and a rf power of 10 dBm the intensity is  $I=0.23$  W/m. We neglect the mechanical losses across the film (about 3 dB for a length  $x=700$   $\mu$ m).  $\Gamma$  can be taken from Fig. 2 and the SAW velocity in the hybrid at  $\sigma=\sigma_m$  was determined both from the finite-element simulations and group delay time measurements. It turns out to be  $v=3730$  m/s. With this input data we calculate an ae current of  $I_{sc}=j_{sc}A=25$   $\mu$ A at a rf power of 10 dBm, which is in good agreement with the measured value in Fig. 2, without the need of any adjustable parameter.

In order to determine the time dependence of the ae current, time-resolved measurements employing pulsed SAW were carried out. A gate bias  $V_g=-3.6$  V was applied between the gate and the 2DES. The ae current was measured via the voltage drop across an Ohmic resistance of 1 k $\Omega$  using an oscilloscope. The result is shown in Fig. 3. At the time when the SAW propagates through the ELO film, the ae current builds up. The propagation time across the film is 190 ns, and thus, smaller than the pulse length. For reversing the SAW direction, again, a reversed signal is measured as predicted.

An alternative experimental approach is the ‘‘open geometry.’’ Here, the ae voltage between two contacts to the 2DES is measured. This geometry does not allow a current to flow, which results in the occurrence of a static ae voltage. With  $j=0$ , Eq. (3) leads to  $E=I\Gamma/n_s e v$ . Then, the ae voltage  $V_{ae}$  across the ELO film of length  $x$  is given by

$$V_{ae} = \int_0^x \frac{I(x)\Gamma}{n_s e v} dx = \frac{\Gamma I_0}{n_s e v} \int_0^x e^{-\Gamma x} dx = \frac{I_0}{n_s e v} (1 - e^{-\Gamma x}). \quad (6)$$

Using the set of sample parameters described above, the evaluation of Eq. (6) results in a very good agreement be-

tween this calculation and our experimental findings over several decades of applied RF power. For example, we obtain a maximum ae voltage of 3.1 V at  $\sigma=\sigma_m$  and  $P=10$  dBm, which is in excellent agreement with the measured value of 3.0 V. However, since at large SAW intensities the ae voltage may become comparable to the gate voltage, the carrier distribution in the 2DES turns out to be affected by pinch-off effects. Therefore, at high acoustic intensities a current measurement in shorted geometry is more reliable.

As we use split-finger multifrequency transducers, we can simultaneously investigate the frequency dependence of the ae current on the same device. Again, the general agreement between our model and the experiment is very good. However, to understand the amplitude of the ae current as a function of frequency in detail, the SAW intensity  $I$ , the different SAW attenuation  $\Gamma$ , and the SAW velocity dispersion in the hybrid have to be taken into account. A detailed analysis including these complications will be presented elsewhere.

In summary, we presented experimental and theoretical results for the acoustoelectric effect in semiconductor/piezoelectric hybrid systems. Combining the advantages of both materials we are able to produce a system that exhibits an unusual large acoustoelectric effect. Voltages up to the order of 10 V and ae currents up to 0.4 mA have been created by the momentum transfer between a strong surface acoustic wave and a high mobility electron system in a semiconductor heterostructure. This could lead to new nonlinear SAW devices with enormously increased signal convolution efficiency compared to conventional SAW convolvers.<sup>10</sup> Apart from the possibility of realizing novel high-frequency devices, our findings clearly demonstrate the applicability of our model to describe complex systems like these hybrids in great detail.

The authors gratefully acknowledge the technical assistance of S. Manus, T. Ostertag, and S. Berek, and many valuable discussions with J. P. Kotthaus, S. Böhm, and C. Rocke. This work has been sponsored in part by the Deutsche Forschungsgemeinschaft and by the German–Israeli Foundation.

<sup>1</sup>K. A. Ingebrigtsen, J. Appl. Phys. **41**, 454 (1970).

<sup>2</sup>A. Wixforth, J. P. Kotthaus, and G. Weimann, Phys. Rev. B **40**, 7874 (1989).

<sup>3</sup>R. L. Willet, R. R. Ruel, K. W. West, and L. N. Pfeiffer, Phys. Rev. Lett. **71**, 3846 (1993).

<sup>4</sup>M. Rotter, C. Rocke, S. Böhm, A. Lorke, A. Wixforth, W. Ruile, and L. Korte, Appl. Phys. Lett. **70**, 2097 (1997).

<sup>5</sup>R. H. Parmenter, Phys. Rev. **89**, 990 (1953).

<sup>6</sup>G. Weinreich and H. G. White, Phys. Rev. **106**, 1104 (1957); G. Weinreich, *ibid.* **107**, 317 (1957).

<sup>7</sup>V. I. Fal’ko, S. V. Meshkov, and S. V. Iordanskii, Phys. Rev. B **47**, 9910 (1993); A. Esslinger, R. W. Winkler, C. Rocke, A. Wixforth, J. P. Kotthaus, H. Nickel, W. Schlapp, and R. Lösch, Surf. Sci. **305**, 83 (1994).

<sup>8</sup>E. Yablonoich, D. M. Hwang, T. J. Gmitter, L. T. Florez and J. P. Harbison, Appl. Phys. Lett. **56**, 2419 (1990).

<sup>9</sup>M. Rotter, A. Wixforth, J. P. Kotthaus, W. Ruile, D. Bernklau, and H. Riechert, Proc. IEEE Ultrasonics Symp., Vol. I, 201, IEEE Cat. No. 97CH36118, New York (1997).

<sup>10</sup>R. B. Thompson and C. F. Quate, Appl. Phys. Lett. **16**, 494 (1970); L. Reindl, H.-W. Wörz, H. P. Grassl, Proc. IEEE Ultrasonics Symp., 85, IEEE Cat. No. 87CH2492-7, New York (1987).